Nucleic Acids Research, 2025, **53**, gkaf698
https://doi.org/10.1093/nar/gkaf698
Molecular and Structural Biology

Temperature-dependent funnel-like DNA folding landscapes

Marc Rico-Pasto [1,2], **Marco Ribezzi-Crivellari** [3], **Felix Ritort** [4,5,6,*]

[1]Unit of Biophysics and Bioengineering, Department of Biomedicine, School of Medicine and Health Sciences, University of Barcelona, C/Casanoves 143, 08036 Barcelona, Spain
[2]Institute for Bioengineering of Catalonia (IBEC), The Barcelona Institute for Science and Technology (BIST), 08028 Barcelona, Spain
[3]École Supérieure de Physique et de Chimie Industrielles (ESPCI), Laboratoire de Biochimie (LBC), 75005 Paris, France
[4]Condensed Matter Physics Department, University of Barcelona, C/Martí i Franquès 1, 08028 Barcelona, Spain
[5]Institut de Nanociència i Nanotecnologia (IN2UB), 08028 Barcelona, Spain
[6]Reial Acadèmia de Ciències i Arts de Barcelona (RACAB), La Rambla 115, E-08002 Barcelona, Spain
[*]To whom correspondence should be addressed. Email: fritort@gmail.com

Abstract

Nucleic acid hybridization in bimolecular and folding reactions is a fundamental kinetic process susceptible to water solvation, counterions, and chemical modifications with intricate enthalpy–entropy compensation effects. Such effects hinder the typically weak temperature dependencies of enthalpies and entropies quantified by the heat capacity change upon duplex formation. Using a temperature-jump optical trap, we investigate the folding thermodynamics and kinetics of DNA hairpins of varying stem sequences and loop sizes in the temperature range of 5–40°C. From a kinetic analysis and using a Clausius–Clapeyron equation in force, we derive the hybridization heat capacity changes ΔC_p per GC and AT bp, finding 36 ± 3 and 29 ± 3 cal/(mol K), respectively. The almost equal values imply similar degrees of freedom arrest upon GC and AT bp formation during duplex formation. Folding kinetics on DNA hairpins of varying loop sizes show that the transition states (TS) in duplex formation have high free energies but low ΔC_p values relative to the native state. Consequently, TS have low configurational entropy in agreement with the funnel-like energy landscape hypotheses. Our study underlines the validity of general principles in the hybridization and folding of nucleic acids determined by the TS's ΔC_p values.

Graphical abstract

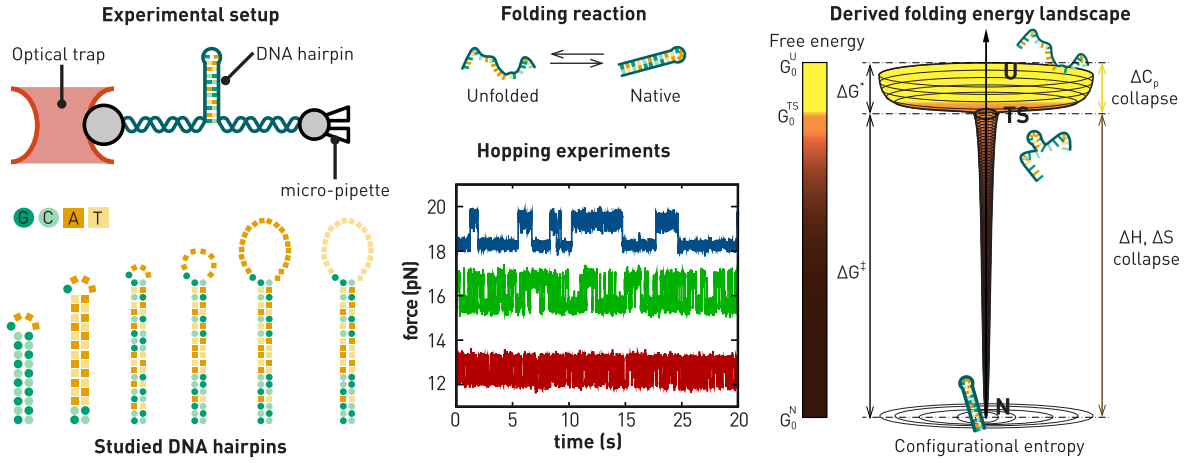

Introduction

A fundamental reaction in nucleic acids is hybridization, the process by which two complementary single strands form a double helix. Hybridization occurs in two ways (Fig. 1A): as a bimolecular reaction by mixing two oligonucleotides A and B to form a duplex AB or as a uni-molecular reaction where a single strand with two complementary regions folds to form a hairpin [1]. Despite the prevalence of such reactions, the thermodynamic characterization of the key kinetic steps remains open. Energy landscapes are a paradigm for

Received: November 24, 2024. **Revised:** June 12, 2025. **Editorial Decision:** July 1, 2025. **Accepted:** July 7, 2025

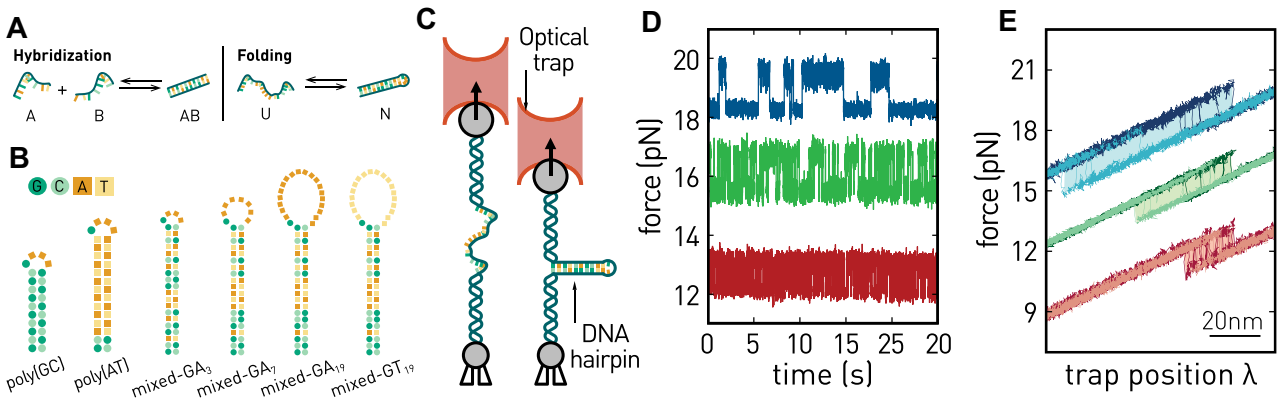

Figure 1. Single-molecule experimental setup. (**A**) Schematic for a hybridization and folding process. (**B**) Cartoon showing the studied DNA sequences. Dark (light) green circles denote guanine (cytosine) bases, and dark (light) squares denote adenine (thymine) bases. (**C**) The hairpin under study is tethered between two polystyrene beads with double-stranded DNA (dsDNA) handles. One bead is captured in the optical trap, while the other is fixed at the tip of a glass micro-pipette. (**D**) Hopping experiments. Force–time traces for the mixed-GA_3 hairpin at three selected temperatures: 6°C (blue), 25°C (green), and 45°C (red). Notice the temperature dependence of the force and timescales of the two force levels (upper level, folded; lower level, unfolded). (**E**) Pulling experiments. Five illustrative force–distance curves for the mixed-GA_3 hairpin at three selected temperatures: 6°C (blue), 25°C (green), and 45°C (red). Dark color curves are unfolding trajectories, while light color curves are folding trajectories. Notice the increase in hysteresis (shaded areas) upon decreasing temperature.

understanding biomolecular reactions, such as unimolecular folding. Reconstructing folding energy landscapes (FELs) requires accurate knowledge of the energy of the conformations explored along a reaction coordinate [2]. Detecting kinetic states along the folding pathway is a main limitation, including transition states (TS) mediating the unfolded and native basins of attraction [3]. It has been suggested that the FEL has a funnel-like shape similar to a golf course. In this picture, the TS lies at the hole's edge while the native state is at the bottom [4, 5]. Heat capacity changes ΔC_p quantify the reduction in degrees of freedom and the structural changes upon folding. Despite bulk methods giving valuable information about native states, they remain inapplicable to derive the energetics of the TS and the FEL. For protein barnase, we have recently measured the ΔC_p values between the TS and the native and unfolded states, highlighting the funnel-like shape of the FEL [6]. Here, we aim to determine the funnel-like features of the FEL in DNA hairpin folding through thermodynamic and kinetic measurements using calorimetric force spectroscopy.

Established techniques for measuring the thermodynamics of hybridization are differential scanning calorimetry (DSC) [7] and isothermal titration calorimetry (ITC) [8]. Previous studies based on DSC suggested that the DNA enthalpy and entropy of hybridization, ΔH_0 and ΔS_0, are temperature-independent. From the relation $\Delta C_p = \partial \Delta H_0/\partial T = (1/T)\partial \Delta S_0/\partial T$, this implies a vanishing ΔC_p upon DNA hybridization [9–11]. However, subsequent studies combining ITC and DSC [12–15] demonstrated that the enthalpy difference measured at low (ITC) and high (DSC) temperatures do not match, proving that $\Delta C_p \neq 0$. In a first approximation, ΔH_0 and ΔS_0 can be expanded around the melting temperature T_m as

$$\Delta H_0(T) = \Delta H_0^m + \Delta C_p\,(T - T_m)\,, \tag{1a}$$

$$\Delta S_0(T) = \Delta S_0^m + \Delta C_p \log\left(\frac{T}{T_m}\right). \tag{1b}$$

with ΔH_0^m and ΔS_0^m the enthalpy and entropy changes at T_m. Hybridization studies on DNA oligonucleotides of varying sequence and length showed that ΔH_0^m and ΔS_0^m for a GC (guanine paired with cytosine) or an AT (adenine paired with thymine) base pair (bp) are different [15–18]. Mikulecky and Feig collected the ΔC_p values per bp measured from differences in the baseline on heat capacity curves [14] and from the linear dependence of ΔH_m versus T_m [14, 19], finding that values per bp fall in the range −30 up to 332 cal/(mol K) depending on oligo sequences, lengths, and experiments carried out [20]. Here, we use calorimetric force spectroscopy to reduce this uncertainty by determining the ΔC_p difference between AT and GC bp in DNA hairpin folding.

Fluorescent single-molecule [21–23] and force-spectroscopy single-molecule experiments (SMEs) allow us to measure folding [24–26] and binding [27–29] energies with kcal/mol accuracy. In SME, force controls the folding transition by modulating the relative stability of the native and unfolded hairpin. SME permits deriving the force-dependent unfolding and folding kinetic rates with high accuracy and reconstructing FELs [30–35]. FELs are commonly investigated using the Bell–Evans (BE) model [36–38] and the diffusive kinetics approach [39–42]. The BE model describes (un)folding transitions as activated jumps over a kinetic barrier that depends on the force. In the diffusive kinetics approach, the folding reaction is a Brownian process in a force-dependent one-dimensional FEL. While free energy differences ΔG_0 ($=\Delta H_0 - T\Delta S_0$) and FEL at room temperature are commonplace, determining folding enthalpies and entropies has remained largely unexplored in SME.

A few groups worldwide have developed instruments capable of controlling temperature using single-molecule fluorescence [43–46] and optical tweezers [47–49]. In contrast to bulk assays like DSC or ITC, where TS have been characterized indirectly by changing the salt conditions, force-spectroscopy experiments allow precise characterization of the FEL by keeping the salt or temperature conditions fixed. In this context, calorimetric force spectroscopy is a valuable resource. Here, we study the FEL of DNA hairpins at different temperatures using calorimetric tweezers by deriving $\Delta S_0(T)$ from the Clausius–Clapeyron equation with force [6, 50]. Moreover, by studying the temperature dependence of the kinetic rates at zero force, we derive the enthalpy and entropy

Table 1. Sequence of the investigated DNA hairpins

Name	Sequence
Poly(GC)	5′-GCGCGCGCGC GAAA GCGCGCGCGC-3′
Poly(AT)	5′-GCATATATATATAT GAAA ATATATATATATGC-3′
Mixed-GA_3	5′-GC**GAG**CCATAATCTCATCTG GAAA C**AGATGAGA**TTATGGCTCGC-3′
Mixed-GA_7	5′-GC**GAG**CCATAATCTCATCTG GAAAAAAA C**AGATGAGA**TTATGGCTCGC-3′
Mixed-GA_{19}	5′-GC**GAG**CCATAATCTCATCTG GAAAAAAAAAAAAAAAAAA C**AGATGAGA**TTATGGCTCGC-3′
Mixed-GT_{19}	5′-GC**GAG**CCATAATCTCATCTG GTTTTTTTTTTTTTTTTTT C**AGATGAGA**TTATGGCTCGC-3′

The loop sequences are highlighted in underline.

differences of the TS relative to the native state ($\Delta H^{\ddagger}$, $\Delta S^{\ddagger}$) and unfolded state (ΔH^{*}, ΔS^{*}) [6]. Determining $\Delta H^{\ddagger}$, $\Delta S^{\ddagger}$, ΔH^{*}, ΔS^{*}, and the corresponding values of $\Delta C_p^{\ddagger}$ and ΔC_p^{*} gives a detailed picture of the temperature-dependent FEL.

To address these questions, we have performed DNA hairpin folding experiments in the temperature range 5–50°C using a temperature-jump optical trap [50, 51]. We have considered two groups of hairpin sequences. First, we have studied GC-rich, AT-rich, and 50% GC-content stem sequences of hairpins ending in a GA_3 tetra-loop. We have determined the temperature-dependent ΔG_0, ΔH_0, ΔS_0, and the ΔC_p values per GC and AT bp with cal/(mol K) accuracy. The second group contains hairpins of fixed stem and variable loop size and composition. This has permitted us to characterize the FEL by measuring the temperature-dependent $\Delta H^{\ddagger}$, $\Delta S^{\ddagger}$, ΔH^{*}, and ΔS^{*}. From there, we derive the ΔC_p values between the TS and the native and unfolded states, confirming the funnel-like shape of the FEL for DNA folding.

Materials and methods

DNA hairpin synthesis

DNA hairpins are synthesized by hybridizing two oligonucleotides [52]: a primary oligo containing the sequence of the hairpin flanked by a single-stranded DNA (ssDNA) handle and a second *splint* oligo. The handles flanking the hairpins are the same for all hairpins, 5′-A G T T A G T G G T G G A A A C A C A G T G C C A G C G C-3′, which hybridize to the complementary splint oligo. After hybridization, two identical dsDNA handles flank the DNA hairpin on each side. Hairpin sequences are summarized in Table 1 and Fig. 1B.

Single-molecule experiments

In SME, molecular constructs are tethered between two polystyrene beads of diameters 3.15 μm (Kisker Biotechnologies) and 2.17 μm (Spherotech, SVP-20-5). The optical trap controls the 3.15 μm bead (bead type I), while the 2.17 μm bead (bead type II) is kept fixed at the tip of a glass micropipette by air suction (Fig. 1C). The 5′-end of one handle is labeled with one biotin, while the 3′-end of the other handle is labeled with a digoxigenin tail. Biotin- and digoxigenin-labeled ends specifically bind to beads coated with streptavidin (type II beads) and anti-digoxigenin (type I beads), respectively. The experiments were done with buffer media containing 10 mM Tris, 1 M NaCl, 1 ml ethylenediaminetetraacetic acid, and 0.01% NaN_3 at pH 7.5.

Hopping experiments

In hopping experiments, the optical trap is kept fixed at different positions to record the thermally activated unfolding and folding transitions from the force signal. For a given trap position or fixed distance between the center of the optical trap and the bead on the micro-pipette, molecules with two states (native and unfolded) present two force levels. The number of released bases in the unfolding of the hairpin determines each force level. When the molecule unfolds (folds), the released (withheld) ssDNA of the hairpin elongates (shortens) the tether extension, resulting in a lower (higher) force (Fig. 1D). Recorded time traces typically span a few minutes at each trap position, allowing us to characterize the unfolding and folding kinetic rates. Figure 1D shows three force–time traces measured at 6°C (blue), 25°C (green), and 45°C (red) for the mixed-GA_3 hairpin.

Pulling experiments

In pulling experiments, the optical trap position λ is repeatedly moved up and down at a constant speed, increasing and decreasing the distance between the molecular construct's ends. Force is ramped between an initial low force where the molecule is folded and a maximum high force where the molecule is unfolded (Fig. 1E). During stretching (dark color curves in Fig. 1E), the unfolding events are observed as sudden force rips in the force versus the distance λ curves. Upon releasing the force, hairpins refold (light color curves in Fig. 1E), and folding transitions are detected as force jumps. The force–distance curves shown in Fig. 1E show two different force branches due to the different elastic responses of the system when the hairpin is in its native or unfolded state. Figure 1E shows five force–distance curves measured at 6°C (blue), 25°C (green), and 45°C (red) for the mixed-GA_3 hairpin.

Temperature-jump optical trap

We have used a temperature-jump optical trap capable of tuning the experimental temperature from 5°C to 50°C [50, 51]. Briefly, the instrument raises the temperature near the optical trap by heating the water solution using a 1435 nm wavelength laser. This laser is collimated at the optical trap position, analogous to Köhler illumination, to heat a 50 μm region where SME are performed. We did Stokes tests after recording the data for each studied molecule to determine the experimental temperature. The temperature inside the chamber at discrete laser powers is determined from the slope of the force versus velocity curves using the Vogel–Fulcher–Tammann equation for water's viscosity. The instrument can be placed in a 25°C temperature-controlled laboratory or inside an icebox with an internal temperature of 5°C. The heating laser raises the temperature from the initial 25°C (or 5°C) to 50°C (or 30°C), allowing us to measure over the full range of 5–50°C.

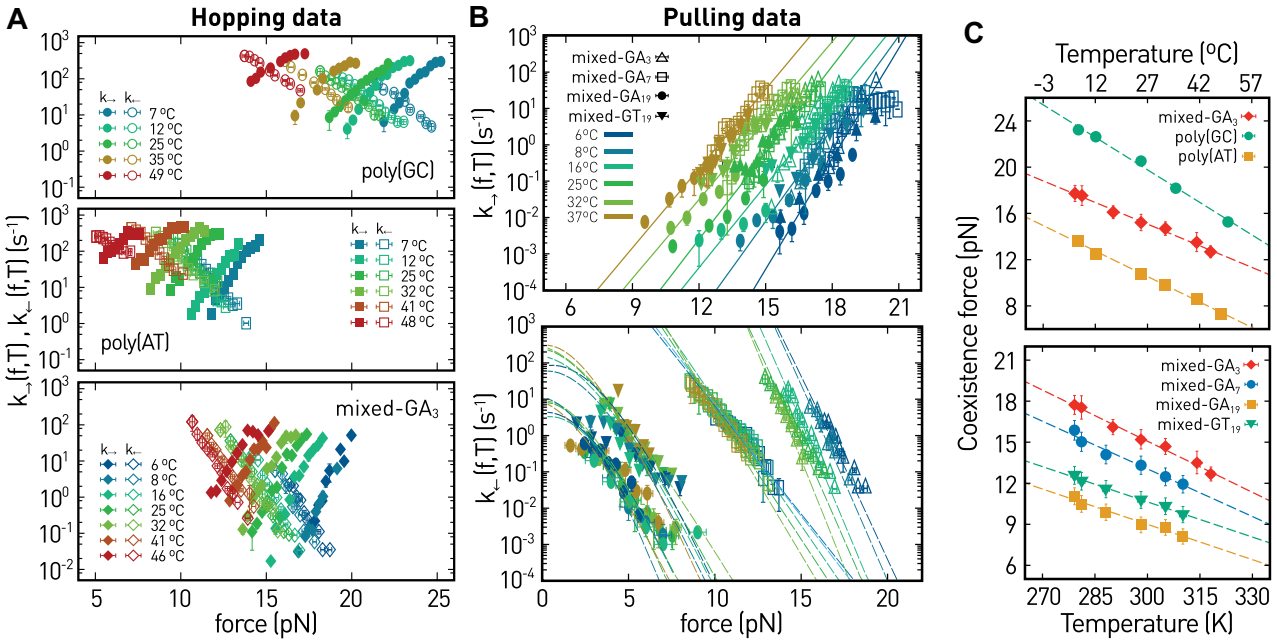

Figure 2. Temperature-dependent kinetic rates. (**A**) Unfolding ($k_{\rightarrow}$, solid symbols) and folding ($k_{\leftarrow}$, empty symbols) kinetic rates for the poly(GC) (top), poly(AT) (middle), and mixed-GA_3 (bottom) hairpins measured at different temperatures. (**B**) Unfolding (top) and folding (bottom) kinetic rates of mixed-GA_3 (diamonds), mixed-GA_7 (circles), mixed-GA_{19} (squares), and mixed-GT_{19} (triangles) at 6°C (dark blue), 8°C (light blue), 16°C (turquoise), 25°C (green), 32°C (khaki), and 37°C (brown). Notice that $k_{\rightarrow}$ overlap for all explored hairpins. In contrast, $k_{\leftarrow}$ for mixed-GA_7, mixed-GA_{19}, and mixed-GT_{19} do not depend on temperature, while $k_{\leftarrow}$ for mixed-GA_3 is weakly T-dependent. (**C**) Coexistence force as a function of temperature for the poly(GC), poly(AT), and mixed-GA_3 (top) and for the mixed-GA_3, mixed-GA_7, mixed-GA_{19}, and mixed-GT_{19} (bottom). The dashed lines are linear fits to determine $\partial f_c/\partial T$, which, combined with equation (8) gives $\Delta S_0(T)$.

Results

We performed hopping experiments for the first three DNA hairpins shown in Table 1. The hairpins are made of different stems ending in a 5′-GAAA-3′ tetra-loop denoted as GA_3. The first hairpin, *poly(GC)*, has a 10-bp stem of five alternating 5′-GC-3′ and 5′-CG-3′ dinucleotide motifs. The second hairpin, *poly(AT)*, has a 14 bp stem of six alternating 5′-AT-3′ and 5′-TA-3′ dinucleotide motifs plus a single 5′-GC-3′ motif preceding the 12 AT bp to prevent fraying of the stem. We designed stems consisting of purine-pyrimidine steps in alternating sequences of dinucleotide motifs to minimize stacking between bases when hairpins are in their unfolded single-stranded form [53]. Finally, the hairpin *mixed-GA_3* has a stem of 20 bp of 50% GC content and has been used to test the consistency of the results obtained for poly(GC) and poly(AT). The stem of the mixed-GA_3 contains three motifs of a few consecutive purines along the ssDNA (GAG, AGA, and GAGA, Table 1 in bold), which are too short to stack in the unfolded state cooperatively [54, 55].

We have also investigated how the loop's length and sequence modify the values of ΔG_0, ΔS_0, ΔH_0, and ΔC_p for hairpins with the same stem sequence as mixed-GA_3. Hairpins are *mixed-GA_7*, *mixed-GA_{19}*, and *mixed-GT_{19}* with GX_n denoting loops of n + 1 bases where G is followed by n bases of type X from 5′ to 3′ (see Table 1). These hairpins do not show hopping in equilibrium conditions within the experimental timescales. Therefore, we derived the force–dependent (un)folding kinetic rates between 5°C and 40°C from non-equilibrium pulling experiments.

Folding free energy, entropy, and enthalpy

We have measured the force- and temperature-dependent unfolding ($k_{\rightarrow}(f, T)$) and folding ($k_{\leftarrow}(f, T)$) kinetic rates to determine $\Delta G_0(T)$, $\Delta S_0(T)$, $\Delta H_0(T)$, and ΔC_p for all hairpins: poly(GC), poly(AT), mixed-GA_3, mixed-GA_7, mixed-GA_{19}, and mixed-GT_{19} hairpins. Let N and U denote the native hairpin and unfolded states, respectively. Thermodynamic changes upon folding are conventionally defined as $\Delta X = X^{\mathrm{U}} - X^{\mathrm{N}}$ with $X = G, S, H, C_p$ with N the initial and U the final states. The unfolded state is a stretched ssDNA polymer if pulled at a given force. In contrast, the unfolded state is a random coil at zero force. Energy differences at zero force will be denoted by the subscript 0, i.e. ΔX_0.

We carried out hopping experiments for poly(GC), poly(AT), and mixed-GA_3 at different force conditions (see the 'Materials and methods' section) and temperatures (5–50°C). Figure 1D shows the first 25 s of a force–time trace measured at 6°C (blue), 25°C (green), and 45°C (red) for mixed-GA_3. Notice that unfolding and folding forces decrease while the hopping frequency increases with temperature. To estimate $k_{\rightarrow}(f, T)$ and $k_{\leftarrow}(f, T)$ from the force–time traces, we calculated the lifetime $\langle\tau\rangle$ of each state,

$$k_{\rightarrow}(f, T) = 1/\langle\tau_N(f, T)\rangle, \tag{2a}$$

$$k_{\leftarrow}(f, T) = 1/\langle\tau_U(f, T)\rangle\ . \tag{2b}$$

Figure 2A shows the unfolding (solid symbols) and folding (empty symbols) kinetic rates for poly(GC) (top), poly(AT) (middle), and mixed-GA_3 (bottom) at different temperatures. Notice that poly(GC) unfolds/folds at higher forces than poly(AT) does, whereas mixed-GA_3 falls in between, indicat-

ing that the energy needed to unfold poly(GC) is higher than poly(AT), even if poly(GC) has a stem of 10 bp, shorter compared to the 14-bp poly(AT). Overall, kinetic rates increase with temperature while the coexistence force f_c, where $k_{\rightarrow}(f_c, T) = k_{\leftarrow}(f_c, T)$, decreases with temperature (Fig. 2C).

The kinetic rates for the different loops have been determined from pulling experiments, Fig. 1E. We measured the survival probabilities of N and U from the force–distance curves at different temperatures using the high-throughput approach introduced in references [42, 56]. Survival probabilities are calculated as follows:

$$P^{\mathrm{N}}_{\rightarrow}(f, T) = 1 - \frac{n(f^{\ddagger} < f)}{\mathbb{N}}, \tag{3a}$$

$$P^{\mathrm{U}}_{\leftarrow}(f, T) = 1 - \frac{n(f^{*} > f)}{\mathbb{N}} \ . \tag{3b}$$

In equation (3a) (equation 3b), $f^{\ddagger}$ (f^{*}) denotes the first unfolding (folding) force event along the unfolding (folding) trajectory. The first unfolding (folding) force is the force value where the molecule transits from $N \rightarrow U$ ($N \leftarrow U$) for the first time in the force–distance curve. Moreover, $n(f^{\ddagger} < f)$ ($n(f^{*} > f)$ is the number of such events below (above) a force f, and $\mathbb{N}$ is the total number of recorded trajectories. Kinetic rates satisfy the master equation:

$$r\frac{dP^{\mathrm{N}}_{\rightarrow}(f, T)}{df} = -k_{\rightarrow}(f, T) \cdot P^{\mathrm{N}}_{\rightarrow}(f, T), \tag{4a}$$

$$r\frac{dP^{\mathrm{U}}_{\leftarrow}(f, T)}{df} = k_{\leftarrow}(f, T) \cdot P^{\mathrm{U}}_{\leftarrow}(f, T)\,, \tag{4b}$$

with r being the pulling rate. We used equations (4a) and (4b) to derive $k_{\rightarrow}(f, T)$ and $k_{\leftarrow}(f, T)$ from the survival probabilities. Figure 2B shows results for mixed-GA_3, mixed-GA_7, mixed-GA_{19}, and mixed-GT_{19}. Notice that in Fig. 2B, colors denote temperatures while symbols indicate loop types. Remarkably, unfolding kinetic rates (top panel) for all sequences overlap at each temperature, i.e. different symbols collapse in a single master curve defined by a color. In contrast, the folding kinetic rates of mixed-GA_7, mixed-GA_{19}, and mixed-GT_{19} (bottom panel) overlap at all temperatures for a given sequence. Therefore, different colors collapse in a single master curve defined by a symbol. An exception is mixed-GA_3 (empty triangles), where folding shows a residual temperature dependence.

Figure 2B (top) demonstrates that the loop barely affects the height of the barrier to unfold, located within the stem of the hairpin preceding the opening of the loop. In contrast, Fig. 2B (bottom) highlights a temperature-independent folding kinetics for the largest loop sizes, i.e. mixed-GA_7, mixed-GA_{19}, and mixed-GT_{19}, demonstrating that folding is an entropy-driven process. Supplementary Fig. S1 shows the unfolding and folding kinetic rates for these hairpins independently. This is not the case for the tetra-loop GA_3 of poly(GC), poly(AT), and mixed-GA_3, where folding rates shift to lower forces upon increasing temperature, Fig. 2A and B (bottom).

Folding free energy

To estimate $\Delta G_0(T)$ from the kinetic rates, we used the detailed balance condition that relates $k_{\rightarrow}(f, T)$ and $k_{\leftarrow}(f, T)$ with the force-dependent folding free energy $\Delta G(f, T)$:

$$\frac{k_{\rightarrow}(f, T)}{k_{\leftarrow}(f, T)} = \exp\left(-\beta \Delta G(f, T)\right), \tag{5}$$

with $\beta = 1/k_B T$, k_B Boltzmann's constant and T the temperature. The force-dependent folding free energy $\Delta G(f, T)$ equals the folding free energy difference between N and U at zero force plus the *elastic work* $\Delta G_{\mathrm{el}}(f, T)$ necessary to stretch the molecule from zero force to force f, i.e. $\Delta G(f, T) = \Delta G_0(T) + \Delta G_{\mathrm{el}}(0 \rightarrow f, T)$. The term $\Delta G_{\mathrm{el}}(0 \rightarrow f, T)$ is given by

$$\Delta G_{\mathrm{el}}(f, T) = -\int_0^f x_U(f', T)df' + \int_0^f x_N(f', T)df' \ , \tag{6}$$

where x_U (x_N) denotes the molecular extension of the unfolded (native) state. The first term is the work gained by extending the ssDNA of the unfolded hairpin extension x_U at force f, while the second term is the work delivered to the system by bringing the extension of the native hairpin x_N from force f to zero force. The extension x_N is the projection of the B-DNA double helix diameter (~2 nm) at the stem's beginning along the pulling axis and is modeled with the freely-jointed chain. Here, the decision to use a kinetic approach rather than the fluctuation theorem stems from the desire to minimize experimental and analytical uncertainties. The kinetic method, grounded in direct measurement of force-dependent kinetic rates, allows us to incorporate elastic contributions through a continuous model and obtain ΔG_0 without relying on extrapolation or indirect estimation [6]. Conversely, FT-based methods require careful subtraction of elastic work after identifying the crossing point in noisy distributions, which can significantly amplify errors. We have assumed that the helix diameter is constant with temperature. Regarding x_U, we calculated this extension using the inextensible worm-like chain model using the Marko–Siggia interpolating formula [57],

$$f = \frac{k_B T}{4L_p}\left(\left(1 - \frac{x}{nd_b}\right)^{-2} + 4\frac{x}{nd_b} - 1\right). \tag{7}$$

In equation (7) x ($\equiv x_U$) is the molecular extension, n is the number of bases, L_{p} is the persistence length, and d_b is the inter-phosphate distance. We used the temperature dependence of L_p and d_b reported in previous experiments under the same experimental conditions [58].

To estimate $\Delta G_0(T)$ from equation (5), we must evaluate $k_{\rightarrow}(f, T)$ and $k_{\leftarrow}(f, T)$ in the same force range to calculate their ratio. But, as we can see in Fig. 2B, the unfolding and folding kinetic rates for the largest loops are measured in different force ranges. To overcome this problem, we adopted the method used in ref. [6]. Briefly, we fitted the logarithm of the measured unfolding kinetic rates to a single quadratic function (dashed lines in Fig. 2B, top) and inferred the folding kinetic rates using equation (5) and different trial values of $\Delta G_0(T)$ (ranging from 0 to 40 kcal/mol). The value of $\Delta G_0(T)$ that best fits data is defined as the trial value that minimizes the χ^2 between the experimental values and the reconstructed folding kinetic rates using equation (5) [dashed lines in Fig. 2B (bottom)]. We have performed the same kinetics analysis for poly(GC), poly(AT), and mixed-GA_3 data shown in Fig. 2A, using the methodology described in Supplementary Fig. S2. We estimate the kinetic rates at zero force, $k^0_{\rightarrow}(T)$ and $k^0_{\leftarrow}(T)$, by extrapolating $k_{\rightarrow}(f, T)$ and $k_{\leftarrow}(f, T)$ to zero force using $\Delta G_0(T)$ and equations (5) and (6). In the next section, we use $k^0_{\rightarrow}(T)$ and $k^0_{\leftarrow}(T)$ to derive the entropy and enthalpy of the TS.

Figure 3A shows the measured values of $\Delta G_0(T)$ for poly(GC), poly(AT), and mixed-GA_3 plotted as symbols, whereas Fig. 3D collects the results for the four mixed hair-

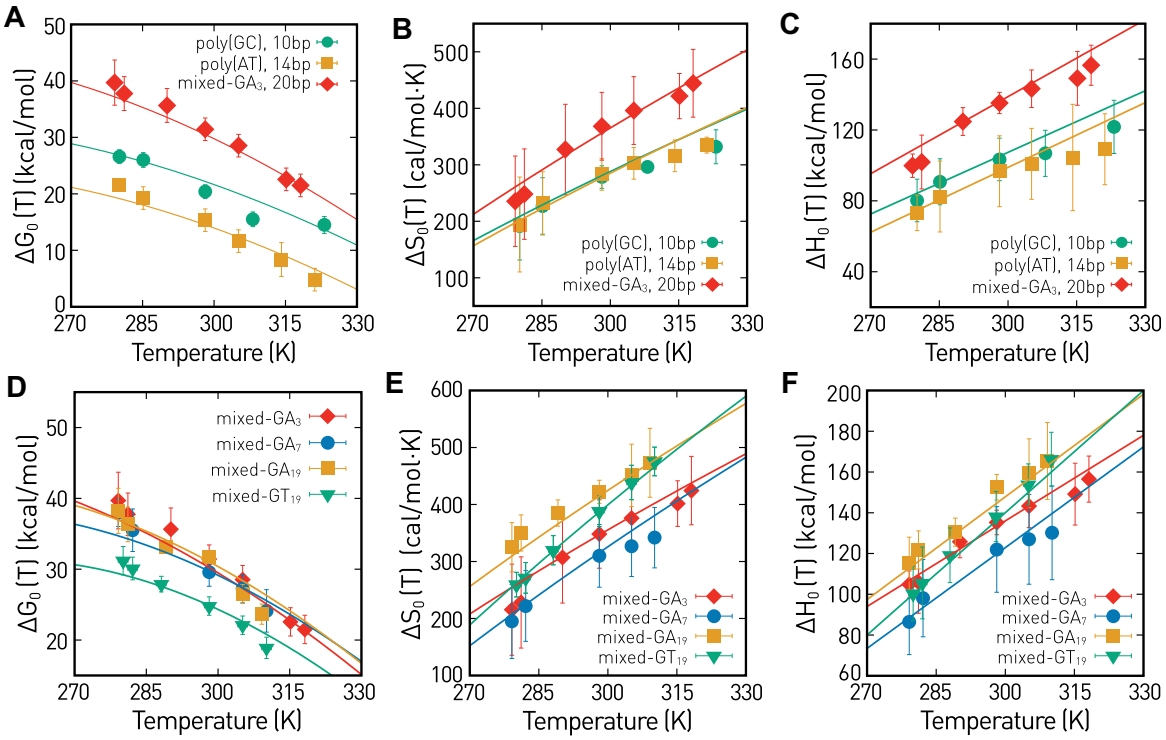

Figure 3. Temperature-dependent folding free energy, entropy, and enthalpy. (**A–C**) $\Delta G_0(T)$, $\Delta S_0(T)$ and $\Delta H_0(T)$ for poly(GC) (green circles), poly(AT) (yellow square), and mixed-GA$_3$ (red diamonds). (**D–F**) $\Delta G_0(T)$, $\Delta S_0(T)$ and $\Delta H_0(T)$ for mixed-GA$_3$ (diamonds), mixed-GA$_7$ (circles), mixed-GA$_{19}$ (squares), and mixed-GT$_{19}$ (triangles) hairpins. The solid lines are fits to the Gibbs's free energy definition [panels (A) and (D)] using the fits to equation (1b) [panels (B) and (E)] and equation (1a) [panels (C) and (F)].

pins. The solid lines in these figures are the Gibbs free energy, $\Delta G_0(T) = \Delta H_0(T) - T\Delta S_0(T)$, using the temperature dependence of $\Delta S_0(T)$ and $\Delta H_0(T)$ derived in the next subsection. Notice that the temperature dependence of $\Delta G_0(T)$ is similar for the mixed-GA$_x$ hairpins due to the small contribution $\lesssim$2 kcal/mol, for all poly(A) loops [59, 60]. Comparing values for the three loop sizes ($x = 3, 7, 19$), we estimate a stacking energy per adenine of ~0.3 kcal/mol, in agreement with bulk studies and SME [61–63].

Finally, we compare the experimental values of $\Delta G_0(T)$ for poly(GC), poly(AT), and mixed-GA$_3$ (Supplementary Fig. S3) and those of mixed hairpins (Supplementary Fig. S4) with the predictions based on the unified oligonucleotide energy parameters [64] where $\Delta C_p = 0$. The agreement is good except for mixed-GT$_{19}$, where the unified oligonucleotide prediction overestimates the stability of the hairpin. Determining ΔC_p from $\Delta G_0(T)$ measurements alone is challenging due to enthalpy–entropy compensation and must be directly measured from $\Delta S_0(T)$ or $\Delta H_0(T)$.

T-dependent folding entropy and enthalpy

We have recently introduced [6] a Clausius–Clapeyron-like equation for calorimetric force spectroscopy to derive $\Delta S_0(T)$ from the force–temperature coexistence line, which reads

$$\Delta S_0(T) = -\frac{\partial f_c(T)}{\partial T}\Delta\lambda(f_c) - \int_0^{f_c(T)} \frac{\partial \Delta\lambda(f', T)}{\partial T} df' \quad , \quad (8)$$

where $\Delta\lambda(f, T) = x_U(f, T) - x_N(f, T)$ is the difference in molecular extension between N and U, and $f_c(T)$ is the force–temperature coexistence line (Fig. 2C). The terms $\Delta\lambda(f, T)$ and $\partial\Delta\lambda(f, T)/\partial T$ are estimated from the ssDNA elasticity [58]. From $\Delta S_0(T)$ and $\Delta G_0(T)$, we obtain $\Delta H_0(T) = \Delta G_0(T) + T\Delta S_0(T)$. $\Delta S_0(T)$ and $\Delta H_0(T)$ values are shown in Fig. 3B and C [poly(GC), poly(AT), mixed-GA$_3$] and in Fig. 3E and F for all mixed hairpins. Results are T-dependent, showing a non-zero ΔC_p for all hairpins. We determined the melting entropy (ΔS_0^m), enthalpy (ΔH_0^m), and ΔC_p by simultaneously fitting the experimental values of $\Delta S_0(T)$ and $\Delta H_0(T)$ to equations (1a) and (1b) with $T_m = \Delta H_0^m/\Delta S_0^m$.

Derivation of ΔC_p values per GC and AT bp, and for the loops

From the results in Fig. 3, we have derived the values of ΔS_0 and ΔH_0 per GC and AT bp, and the loop contribution: $\Delta S_0^{GC}(T)$, $\Delta S_0^{AT}(T)$, and $\Delta S_0^{loop}(T)$; and for the enthalpy: $\Delta H_0^{GC}(T)$, $\Delta H_0^{AT}(T)$, and $\Delta H_0^{loop}(T)$. In line with the nearest-neighbor model, we consider that the contribution of the loop to ΔS_0 is additive, $\Delta S_0(T) = \Delta S_0^{stem}(T) + \Delta S_0^{loop}(T)$ and equally for the enthalpy. For ΔS_0^{stem}, we also assume additivity of individual GC and AT bp contributions, $\Delta S_0^{stem}(T) = n_{GC}\Delta S_0^{GC}(T) + n_{AT}\Delta S_0^{AT}(T)$ with n_{GC} and n_{AT} the number of GC and AT bp in the stem. For hairpins with a given loop sequence the entropies $\Delta S_0^{GC}(T)$, $\Delta S_0^{AT}(T)$, and $\Delta S_0^{loop}(T)$ can be derived from $\Delta S_0(T)$, and analogously for the enthalpies.

Poly(GC), poly(AT), and mixed-GA$_3$ share the same GA$_3$ tetra-loop with $n_{GC} = 10$, 2, 10 and $n_{AT} = 0$, 12, 10, respectively. The values of $\Delta S_0(T)$ and $\Delta H_0(T)$ used in the analysis are shown as continuous lines in Fig. 3B and C. The results for $\Delta S_0^{GC}(T)$, $\Delta S_0^{AT}(T)$, and $\Delta S_0^{loop}(T)$ and the corresponding enthalpies are shown in the Supplementary Fig. S5. By fitting them to the general temperature behavior defined by equations (1a) and (1b), we derive ΔS_0^m and ΔH_0^m at the melting

Table 2. Entropy and enthalpy at T_m, and ΔC_p and T_m

	ΔS_0^m(cal/mol K)	ΔH_0^m(kcal/mol)	ΔC_p(cal/mol · K)	T_m(°C)
poly(GC)	480 ± 20	170 ± 20	1160 ± 110	81 ± 3
poly(AT)	430 ± 20	144 ± 10	1220 ± 120	64 ± 3
mixed-GA_3	618 ± 40	220 ± 20	1450 ± 130	83 ± 5
GC bp	24 ± 1	10 ± 1	36 ± 3	140 ± 20
AT bp	14 ± 1	5 ± 1	29 ± 3	90 ± 9
GA_3-loop	160 ± 20	50 ± 5	800 ± 100	39 ± 4
mixed-GA_3	650 ± 40	231 ± 20	1400 ± 140	83 ± 5
mixed-GA_7	649 ± 20	234 ± 8	1648 ± 120	87 ± 5
mixed-GA_{19}	585 ± 50	210 ± 6	1680 ± 165	67 ± 3
mixed-GT_{19}	605 ± 48	212 ± 13	2000 ± 90	74 ± 3
GA_7-loop	295 ± 20	96 ± 10	998 ± 100	50 ± 20
GA_{19}-loop	323 ± 20	102 ± 10	1030 ± 100	40 ± 20
GT_{19}-loop	294 ± 20	87 ± 10	1350 ± 100	30 ± 10

temperature T_m, and the ΔC_p values per GC and AT bp, and for the GA_3 tetra-loop. Fitting parameters are shown in Table 2, rows 4–6. We obtain $\Delta C_p^{GC} = 36 \pm 3$ cal/(mol K), $\Delta C_p^{AT} = 29 \pm 3$ cal/(mol K), and $\Delta C_p^{GA_3} = 800 \pm 100$ cal/(mol K). Notice that the latter is larger than ΔC_p^{stem} for these hairpins: ∼360 cal/(mol K) for poly(GC); ∼420 cal/(mol K) for poly(AT); and ∼650 cal/(mol K) for the mixed stem. This shows that the major contribution to ΔC_p comes from loop formation.

Transition-state characterization

To elucidate how the loop affects the FEL (Fig. 4A), we derived the T-dependent entropy and enthalpy of the TS relative to N and U. The notation for these differences is $\Delta S^{\ddagger} = S^{TS} - S^{N}$ and $\Delta H^{\ddagger} = H^{TS} - H^{N}$, and similarly for TS and U: $\Delta S^{*} = S^{TS} - S^{U}$ and $\Delta H^{*} = H^{TS} - H^{U}$. At a given force f and temperature T, the kinetic barriers $\Delta G^{\ddagger}$ and ΔG^{*} define the unfolding and folding Arrhenius rates,

$$k_{\rightarrow}(f,T) = k_a \cdot \exp\left(-\frac{\Delta G^{\ddagger}(f,T)}{k_B T}\right), \tag{9a}$$

$$k_{\leftarrow}(f,T) = k_a \cdot \exp\left(-\frac{\Delta G^{*}(f,T)}{k_B T}\right), \tag{9b}$$

where k_a is an attempt rate, and

$$\Delta G^{\ddagger}(f,T) = \Delta H^{\ddagger}(f,T) - T\Delta S^{\ddagger}(f,T) \tag{10a}$$

$$\Delta G^{*}(f,T) = \Delta H^{*}(f,T) - T\Delta S^{*}(f,T). \tag{10b}$$

Equations (9a) and (9b) satisfy the detailed balance condition [equation (5)], with $\Delta G(f, T) = \Delta G^{\ddagger}(f, T) - \Delta G^{*}(f, T)$, and equivalent definitions for $\Delta S(f, T)$ and $\Delta H(f, T)$. The (un)folding kinetic rates at zero force, $k^0_{\rightarrow}(T)$ and $k^0_{\leftarrow}(T)$, depend on the enthalpic and entropic barriers to (un)fold as

$$k^0_{\rightarrow}(T) = k_a \cdot \exp\left(\frac{\Delta S^{\ddagger}_0(T)}{k_B} - \frac{\Delta H^{\ddagger}_0(T)}{k_B T}\right) \tag{11a}$$

$$k^0_{\leftarrow}(T) = k_a \cdot \exp\left(\frac{\Delta S^{*}_0(T)}{k_B} - \frac{\Delta H^{*}_0(T)}{k_B T}\right), \tag{11b}$$

where $\Delta S^{\ddagger}_0$, ΔS^{*}_0, $\Delta H^{\ddagger}_0$, and ΔH^{*}_0 are the entropy and enthalpy of the TS relative to N and U at zero force. Notice that $\Delta S_0 = \Delta S^{\ddagger}_0 - \Delta S^{*}_0$ and $\Delta H_0 = \Delta H^{\ddagger}_0 - \Delta H^{*}_0$.

To derive the T-dependence of $\Delta S^{\ddagger}_0$, $\Delta H^{\ddagger}_0$, ΔS^{*}_0, and ΔH^{*}_0, we combine equations (11a) and (11b) with equations (1a) and (1b). We proceed in two steps explained in the next subsections. First, we derive the attempt rate k_a combining the continuous effective barrier approach (CEBA) and the nearest-neighbor model. Next, we use the value of k_a to fit the extrapolated kinetic rates at zero force shown in Fig. 4 to equations (11a) and (11b), estimating $\Delta S^{\ddagger}_0(T)$, $\Delta S^{*}_0(T)$, $\Delta H^{\ddagger}_0(T)$, and $\Delta H^{*}_0(T)$.

Derivation of the attempt rate k_a

In Eyring's and Kramers's theories, k_a is predicted to vary linearly with T, ∼13% in our temperature range of 5–50°C. This is a small change compared to the exponential dependence of the activation energies in equations (9a) and (9b). Therefore, we assume k_a to be T-independent.

We have applied the CEBA [42, 56] to estimate k_a from the unfolding rates $k_{\rightarrow}(f, T)$. In CEBA, folding is described as a diffusive process in a force- and temperature-dependent FEL, $\Delta G_m(f, T)$, defined as the free energy difference or work necessary to unzip m bp starting from the beginning of the stem (hairpin cartoons in Fig. 4a). Therefore, m defines the reaction coordinate of the FEL. From equation (9a) we have

$$\log(k_{\rightarrow}(f,T)) = -\frac{\Delta G^{\ddagger}(f,T)}{k_B T} + \log(k_a) \quad . \tag{12}$$

The CEBA gives an analytic expression for $\Delta G^{\ddagger}(f, T)$ in terms of the $\Delta G_m(f, T)$,

$$\frac{\Delta G^{\ddagger}(f,T)}{k_B T} = \log\left(\sum_{m=0}^{M}\sum_{m'=0}^{m} e^{\left(\frac{\Delta G_m(f,T) - \Delta G_{m'}(f,T)}{k_B T}\right)}\right). \tag{13}$$

The double sum in equation (13) runs the intermediate hairpin configurations labeled by m and m', with M the total number of bp in hairpin's stem. In equation (13), $\Delta G_m(f, T) = \Delta G_m(0, T) + \Delta G^m_{el}(f, T)$ with $\Delta G_m(0, T)$ equal to the folding energy at zero force and $\Delta G^m_{el}(f, T)$ the energy cost to stretch the partially unzipped hairpin. The nearest-neighbor energy values $\Delta G_m(0, T)$ are obtained either from the unified oligonucleotide database [59, 60] or from the single-DNA unzipping data [65, 66]. The elastic term $\Delta G^m_{el}(f, T)$ equals the energy required to stretch $2m$ bases of ssDNA of the unpaired strands minus the entropy cost of orienting the diameter of the stem along the force axis (equation 6).

To estimate k_a for the different hairpins, we matched the experimental values of $\log(k_{\rightarrow}(f, T))$ in Fig. 2 with those pre-

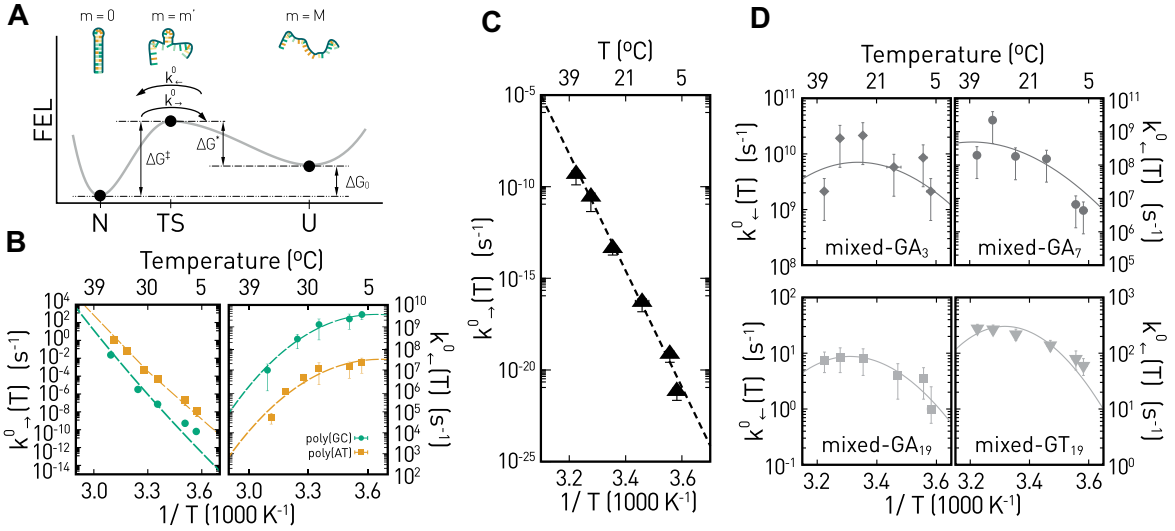

Figure 4. Temperature-dependent kinetic rates at zero force. (**A**) Schematics of a 1D folding free energy landscape highlighting the folding energy ΔG_0 and the energy difference at TS relative to N, $\Delta G^{\ddagger}$, and U, ΔG^{*}. (**B**) Unfolding (left) and folding (right) kinetic rate at zero force for the poly(GC) (top) and poly(AT) (bottom) hairpins. The lines are fits to equations (11a) and (11b). (**C**) Unfolding kinetic rate at zero force considering the four mixed hairpins. The dashed line is a fit to equation (11a). (**D**) Folding kinetic rate at zero force for the mixed-GA_3 (top, left), mixed-GA_7 (top, right), mixed-GA_{19} (bottom, left), and mixed-GT_{19} (bottom, right) hairpins. Lines are fits to equation (11b). Notice that in all cases $k^0_{\rightarrow}(T)$ changes by >10 orders of magnitude, whereas $k^0_{\leftarrow}(T)$ changes over three orders of magnitude at most, in the same temperature range.

dicted by equations (13) and equation (12) at $T = 25^{\circ}$C. We get $k_a = 6 \times 10^{10}$ s^{-1} and $k_a = 5 \times 10^{7}$ s^{-1} for poly(GC) and poly(AT), respectively. For all mixed hairpins, the $k_{\rightarrow}(f, T)$ overlap at $T = 25^{\circ}$C (medium green symbols in Fig. 2B, top) with a common loop-independent $k_a \sim 6 \times 10^{3}$ s^{-1}. These results demonstrate that the barrier to unfolding $\Delta G^{\ddagger}(f, T)$ is unaffected by the loop because the TS is located within the stem preceding the opening of the loop.

Derivation of the enthalpies, entropies, and ΔC_p of the TS

Knowing k_a, we can fit $k^0_{\rightarrow}(T)$ and $k^0_{\leftarrow}(T)$ to equations (11a) and (11b) by imposing the temperature dependence of $\Delta S^{\ddagger}_0(T)$, $\Delta H^{\ddagger}_0(T)$, ΔS^{*}_0, and $\Delta H^{*}_0(T)$, with a finite $\Delta C^{\ddagger}_p$ and ΔC^{*}_p using equations (1a) and (1b) with a single T_m,

$$\Delta H^{\ddagger(*)}_0(T) = \Delta H^{\ddagger(*)}_m + \Delta C^{\ddagger(*)}_p (T - T_m) \tag{14a}$$

$$\Delta S^{\ddagger(*)}_0(T) = \Delta S^{\ddagger(*)}_m + \Delta C^{\ddagger(*)}_p \log\left(\frac{T}{T_m}\right) . \tag{14b}$$

The fits give the melting entropies ($\Delta S^{\ddagger}_m$, ΔS^{*}_m) and enthalpies ($\Delta H^{\ddagger}_m$, ΔH^{*}_m) of TS relative to N and U. Moreover, we also determined the heat capacity changes $\Delta C^{\ddagger}_p$ and ΔC^{*}_p. For convenience, we take them positive by defining $\Delta C^{\mathrm{N-TS}}_p = C^{TS}_p - C^{\mathrm{N}}_p \equiv \Delta C^{\ddagger}_p$, between TS and N, and $\Delta C^{\mathrm{TS-U}}_p = C^{U}_p - C^{TS}_p \equiv -\Delta C^{*}_p$ between TS and U. By definition, $\Delta C_p = \Delta C^{\mathrm{TS-U}}_p + \Delta C^{\mathrm{N-TS}}_p$.

Figure 4B–D shows the experimentally derived (un)folding kinetic rates at zero force, $k^0_{\rightarrow}(T)$ and $k^0_{\leftarrow}(T)$, as a function of the inverse of the temperature as symbols, and the fits to equations (11a) and (11b) as lines. Figure 4B shows results for poly(GC) and poly(AT), and Fig. 4C and D for mixed-GA_3, mixed-GA_7, mixed-GA_{19}, and mixed-GT_{19}. We remind the reader that the unfolding kinetic rates do not depend on loop size and composition (Fig. 2B). Therefore, the results for $k^0_{\rightarrow}(T)$ shown in Fig. 4C have been obtained by taking the $k_{\rightarrow}(f, T)$ of all mixed hairpins as a single dataset at each temperature.

Notice that $k^0_{\rightarrow}(T)$ is almost linear in the explored temperature range (left panels in Fig. 4B and C). In contrast, $k^0_{\leftarrow}(T)$ exhibits a curvature for all explored hairpins (right panels in Fig. 4B and D). The different behaviors reveal that $\Delta C^{\mathrm{N-TS}}_p$ is systematically smaller than $\Delta C^{\mathrm{TS-U}}_p$, as ΔC_p is the parameter that determines the temperature dependence of enthalpies and entropies in equations (14a) and (14b) and the curvature of the Arrhenius plots, $\log(k)$ versus $1/T$. Interestingly, the folding rates for mixed-GT_{19} hairpin are faster than those for mixed-GA_{19}, indicating that the poly(T) loop is easier to bend upon forming the hairpin stem, increasing the folding rate. The linearity of log-normal Arrhenius plots for unfolding and the curvature of the corresponding plots for folding has also been observed in protein folding studies in bulk [67–69] and SMEs [6].

The measured ΔS_m, ΔH_m at the melting temperature T_m, and the ΔC_p values are summarized in Table 3. For the mixed hairpins, the common kinetic rates $k^0_{\rightarrow}(T)$ shown in Fig. 4C have been used to derive the N-TS parameters (Table 3, third row). Table 3 shows that $\Delta H^{\ddagger}_m > \Delta H^{*}_m$, $\Delta S^{\ddagger}_m > \Delta S^{*}_m$, whereas $\Delta C^{\mathrm{N-TS}}_p < \Delta C^{\mathrm{TS-U}}_p$. For the mixed hairpins, $\Delta C^{\mathrm{TS-U}}_p$ increases with the loop size (Table 3, rows 6–9). Finally, $\Delta C^{\mathrm{TS-U}}_p$ is larger for the pyrimidine loop (mixed-GT_{19}, ninth row) as compared to the purine loop (mixed-GA_{19}, eighth row). For the largest loops, Table 3 highlights that $\Delta C_p = \Delta C^{\mathrm{TS-U}}_p + \Delta C^{\mathrm{N-TS}}_p$ with $\Delta C^{\mathrm{TS-U}}_p \gg \Delta C^{\mathrm{N-TS}}_p$. Similar inequalities have been found for protein barnase [6], where it was hypothesized that the TS has the properties of a dry-molten globule structurally similar to the native state but with loosely packed side chains [70–72]. The formation of the large loop in DNA hairpins is reminiscent of the stabilization of the dry-molten globule in protein folding.

Table 3. TS entropy, enthalpy, and free energies at the T_m values shown in Table 2, and ΔC_p

	$\Delta S^{\ddagger}_m$(cal/mol · K)	$\Delta H^{\ddagger}_m$(kcal/mol)	$\Delta G^{\ddagger}_m$(kcal/mol)	$\Delta C_p^{\mathrm{N-TS}}$
poly(GC)	320 ± 20	121 ± 10	8 ± 1	350 ± 40
poly(AT)	280 ± 15	96 ± 10	1.6 ± 0.5	420 ± 20
mixed-all	416 ± 25	156 ± 7	8 ± 1	620 ± 50
	ΔS^{*}_m(cal/mol · K)	ΔH^{*}_m(kcal/mol)	ΔG^{*}_m(kcal/mol)	$\Delta C_p^{\mathrm{TS-U}}$
poly(GC)	−236 ± 12	−73 ± 4	11 ± 1	810 ± 30
poly(AT)	−147 ± 25	−48 ± 10	1.6 ± 0.2	800 ± 40
mixed-GA_3	−131 ± 40	−45 ± 12	4 ± 1	811 ± 40
mixed-GA_7	−133 ± 30	−45 ± 10	5 ± 1	1028 ± 30
mixed-GA_{19}	−169 ± 19	−49 ± 10	9 ± 1	1064 ± 40
mixed-GT_{19}	−205 ± 50	−61 ± 20	10 ± 1	1380 ± 100

Note: $\Delta X^{\ddagger} = X^{\mathrm{TS}} - X^{\mathrm{N}}$ and $\Delta X^{*} = X^{\mathrm{TS}} - X^{\mathrm{U}}$.

Discussion

We have measured DNA hairpin unfolding and folding kinetic rates between 5°C and 50°C to unravel the thermodynamic features of their FELs. Six hairpin sequences of different GC versus AT content in the stem (poly(GC), poly(AT), and mixed-GA_3) and different loop sizes (mixed-GA_7, mixed-GA_{19}, and mixed-GT_{19}) have been investigated using a temperature jump optical trap [6, 50, 51].

We have combined the detailed balance equation (5) with the Clausius–Clapeyron-like equation (8), and thermodynamic relations (1a) and (1b), to derive $\Delta G_0(T)$, $\Delta S_0(T)$, $\Delta H_0(T)$, and ΔC_p from the kinetics rates. Assuming additivity for the energy of base pairing and loop formation, we have estimated ΔC_p values per GC and AT bp and for the different loops. At this description level, the number of energy parameters for duplex formation reduces to the single GC and AT bp values rather than the ten energy parameters of the nearest-neighbor model. Melting temperatures, entropy, and enthalpy values per GC and AT bp are summarized in rows 4 and 5 of Table 2. We find that enthalpies and entropies per GC bp roughly double the values for AT bp (Supplementary Fig. S5). In contrast, ΔC_p values are compatible within errors, $\Delta C_p^{\mathrm{GC}} = 36 \pm 3$ cal/(mol K), and $\Delta C_p^{\mathrm{AT}} = 29 \pm 3$ cal/(mol K), suggesting that similar degrees of freedom arrest upon GC and AT bp formation during stem hybridization. For the loops, ΔC_p values increase with loop's size, from $\Delta C_p^{\mathrm{GA_3}} = 800 \pm 100$ cal/(mol K) to $\Delta C_p^{\mathrm{GA_{19}}} = 1030 \pm 100$ cal/(mol K) for the largest GA_{19} icosa-loop (rows 6, 11, and 12 of Table 2). Interestingly, $\Delta C_p^{\mathrm{GA_{19}}}$ is smaller than $\Delta C_p^{\mathrm{GT_{19}}} = 1350 \pm 100$ cal/(mol K), rows 12 and 13 of Table 2, suggesting that poly(A) stacking of the GA_{19} loop further stabilizes a helix-like structure like has been observed in poly(A) (adenylic) duplexes [74]. Our study shows that ΔC_p values are important for accurate melting temperature predictions. We compared our values with the predicted folding energy based on calorimetry experiments [59, 60] where the $\Delta C_p = 0$ assumption results in straight lines for $\Delta G(T)$ (Supplementary Figs S2 and S3). While the lines pass over the data across the temperature range, they do not reproduce the curvature in $\Delta G(T)$, a consequence of the temperature-dependent ΔH, ΔS and the non-zero ΔC_p, as shown in Fig. 3A and D. The relative weight of the ΔC_p term in equations (1a) and (1b) relative to the full $\Delta G_0(T)$ is ∼10% in the vicinity of T_m increasing up to 50% at 5°C (Supplementary Fig. S6).

To elucidate the main features of the FEL, we characterize the TS using equations (11a) and (11b). We have derived $\Delta C_p^{\mathrm{N-TS}}$ and $\Delta C_p^{\mathrm{TS-U}}$ and the TS entropies and enthalpies at T_m: $\Delta S^{\ddagger}_m$, $\Delta H^{\ddagger}_m$, ΔS^{*}_m, and ΔH^{*}_m. Results are summarized in Table 3. We notice that $\Delta C_p^{\mathrm{N-TS}}$ is the same for the four mixed hairpins (row 3, Table 3), but $\Delta C_p^{\mathrm{TS-U}}$ increases with loop size (rows 6–9, Table 3) implying that loop formation constitutes the TS and the rate-limiting step for hairpin folding. This interpretation aligns with the values of $\Delta C_p^{\mathrm{TS-U}}$ for poly(GC), poly(AT), and mixed-GA_3 [∼800 cal/(mol K), rows 4–6 in Table 3], which match the ΔC_p value for the loop, $\Delta C_p^{\mathrm{GA_3}} = 800 \pm 100$ cal/(mol K) (row 6, Table 2). Moreover, the absolute values $|\Delta H^{*}_m|$ between TS and U for poly(GC), poly(AT), and mixed-GA_3 (rows 4–6, Table 3) agree with the loop value $\Delta H_0^{\mathrm{GA_3}}(T_m) = 50 \pm 5$ kcal/mol.

By comparing rows 1–3 and 4–9 in Table 3, we observe that $\Delta S^{\ddagger}_m$ and $\Delta H^{\ddagger}_m$ (both positive) are two-three times larger than $|\Delta H^{*}_m|$ and $|\Delta S^{*}_m|$. In contrast, $\Delta C_p^{\mathrm{TS-U}}$ is twice $\Delta C_p^{\mathrm{N-TS}}$, indicating that the main reduction in the configurational entropy occurs from U to TS. To quantify which contribution, ‡ or *, is predominant upon folding, we define kinetic fragilities for entropies, enthalpies, and ΔC_p,

$$\mu_{\Delta X} = \frac{\Delta X^{\ddagger} + \Delta X^{*}}{\Delta X^{\ddagger} - \Delta X^{*}}, \tag{15}$$

where ΔX stands for ΔS, ΔH, and ΔC_p calculated at T_m (nota bene: $\Delta C_p^{*} = -\Delta C_p^{\mathrm{TS-U}}$). These kinetic fragilities are the equivalent of mechanical fragilities, defined in terms of the molecular extension of the TS relative to N and U [56]. Folding is a heat-delivering exothermic reaction driven by hydrogen bonding and base stacking. The kinetic fragility for ΔH and ΔS defines the relative heat delivered in the two steps, first from U to TS and next from TS to N. By definition, the quantity $\mu_{\Delta X}$ ranges between −1 and 1 corresponding to the limits $\mu_{\Delta S}, \mu_{\Delta H} \to -1$, where most heat is released from U to TS, and $\mu_{\Delta S}, \mu_{\Delta H} \to 1$, where most heat is released from TS to N. In the intermediate case $\mu_{\Delta S}, \mu_{\Delta H} \sim 0$, equal amounts of heat are dissipated in the two steps. In contrast, ΔC_p quantifies the arresting of the number of degrees of freedom Δn and the reduction of the configurational entropy as per the equipartition law, $\Delta C_p = k_B \Delta n/2$, giving $\Delta n = 1$ per cal/(mol K) unit of ΔC_p. Correspondingly, $\mu_{\Delta C_p}$ defines the degree of structural similarity of TS to N and U. If $\mu_{\Delta C_p} \to -1$, the largest configurational entropy change occurs between U and TS; therefore, the TS is structurally similar to N. In the opposite case, $\mu_{\Delta C_p} \to 1$ and the TS is structurally similar to U. Figure 5A shows the

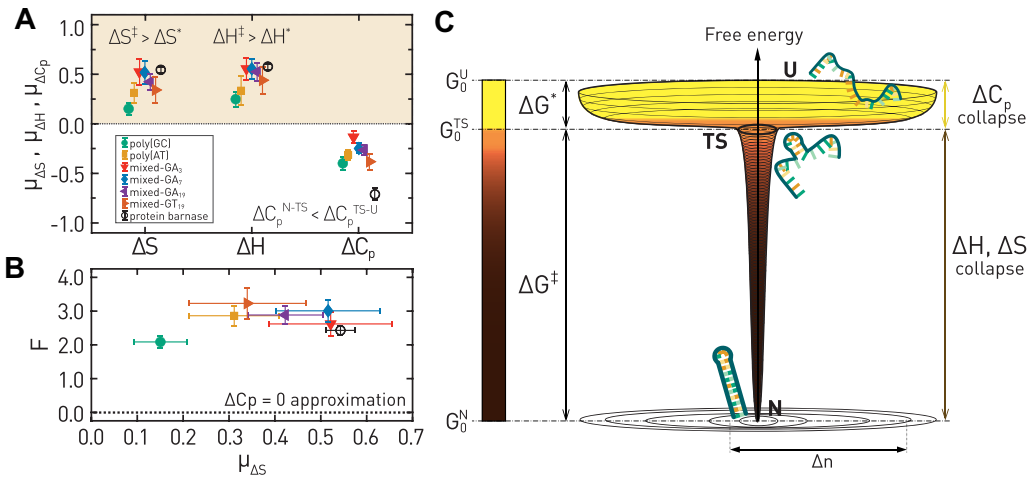

Figure 5. Thermodynamic and kinetic fragilities and FEL. (**A**) Kinetic fragilities defined in equation (15) for the DNA hairpins and protein barnase for comparison (empty black circle). Note that $\mu_{\Delta S} > 0$ and $\mu_{\Delta H} > 0$ while $\mu_{\Delta C_p} < 0$, indicating a large configuration change between TS and U. (**B**) Thermodynamic fragility at T_m, equation (16), versus $\mu_{\Delta S}$. $F \sim$ 2–3 for all molecules, comparable to the values for glass-forming liquids, $F \sim 2$ [73]. (**C**) 3D funnel free energy landscape highlighting N, TS, and U. The color palette grades the free energy difference from U (light color) to N (dark color). The distance relative to N in the orthogonal plane equals Δn (lower black double arrow).

kinetic fragilities for all hairpins compared to results for protein barnase obtained in [6] (empty black circles). We find that $\mu_{\Delta S} > 0$ and $\mu_{\Delta H} > 0$ while $\mu_{\Delta C_p} < 0$, highlighting that the folding process proceeds in two steps: in the first step, the formation of TS from U is characterized by a large configurational entropy loss; in the second step, a large enthalpy and entropy change drives the collapse from TS to N. Indeed, for proteins we get a more negative $\mu_{\Delta C_p}$ compared to DNA hairpins, due to the higher complexity of proteins. The 20 amino acids of proteins versus the four bases of DNA may have produced a steepest funnel for proteins in the light of evolutionary forces. Therefore, the value of $\mu_{\Delta C_p}$ does not necessarily reflect the secondary versus tertiary order of the native structure, but rather the structural similarity of the TS to the native state. This feature should be common to all biomolecules that form native structures stabilized by weak bonds.

Molecular folding is reminiscent of glass formation and crystallization in liquids. If cooled sufficiently fast, liquids freeze into a glass, a disordered solid form of matter of free energy, entropy, and enthalpy higher than the crystal [73, 75, 76]. In this regard, the supercooled metastable state in glasses is analogous to a non-productive TS in molecular folding, which does not crystallize on observable timescales. In glass-forming liquids, the thermodynamic fragility F is defined by the dimensionless ratio $\Delta C_p/\Delta S_m$ where differences Δ are measured between the crystal and the liquid,

$$F = \frac{\Delta C_p}{\Delta S_m}. \qquad (16)$$

Figure 5B shows $F \sim$ 2–3 for all studied molecules. The horizontal dotted line $F = 0$ corresponds to the $\Delta C_p = 0$ approximation adopted in hybridization studies. Glass-forming liquids exhibit similar values $F \sim 2$ [73], revealing that molecular folding and glass formation are analogous processes.

In fact, at zero force, the TS of the funnel-like landscape cannot be described by simplistic quartic-like potentials with two minima (folded and unfolded states) and one maximum (TS) along the molecular extension, usually employed to model folding and unfolding around the coexistence region where hopping is observed. In particular, at the coexistence force f_c, where the unfolded and folded states are equally populated, the TS is located along the hairpin stem, typically around its middle point [30, 56]. The TS position changes with force as predicted by the Hammond–Leffler postulate, i.e. it moves against the state that is thermodynamically favored by the force. If force decreases, the folded state is stabilized, so the TS moves upwards along the stem and towards the loop. If force increases, the opposite occurs, and the TS moves towards the beginning of the hairpin. The TS ceases above the upper spinodal and below the lower spinodal transition forces, $f^>$ and $f^<$, where the TS forms a saddle point. In the protein folding context, this fact has given rise to alternative potentials inspired by Landau theory of phase transitions, the so-called downhill scenario [77] or by entropic spring models [78] (see Supplementary data and Supplementary Fig. S8 for more details). In line with the previous paragraph, molecular folding at zero force is reminiscent of the nucleation problem and crystallization in liquids. Upon quenching a liquid from high to low temperatures, the nucleating barrier and TS to solidification are set by the growth of a solid droplet of critical size. For DNA hairpin folding, the formation and subsequent transient stabilization of the hairpin loop determine the critical steps to nucleation and folding.

Summing up, we interpret molecular folding as a two-step process in a funnel-like FEL, which is illustrated in Fig. 5C as a 3D plot. First, a large reduction in the configurational entropy, measured as a large $\Delta C_p^{\mathrm{TS-U}}$, occurs during the stabilization of the loop to reach the TS from U. Second, a significant enthalpic and entropic change occurs in the collapse from TS to N due to the rezipping of the stem. A substantial ΔC_p reduction upon forming the TS is reminiscent of what has been observed in protein barnase [6], supporting a funnel-like FEL scenario for DNA folding at zero force. The vertical axis in Fig. 5C stands for the free energy of the hairpin. Moreover, the 2D planisphere (bottom) illustrates the reduction in the degrees of freedom Δn relative to N and ΔC_p upon folding. The purpose of the 2D planisphere is to emphasize the large number of degrees of freedom in the folding pathway, far beyond the 1D reductionistic view represented by the number of native contacts. In the 3D plot of the FEL in Fig. 5C, the

color palette grades the vertical axis for the free energy from U (light color) to N (dark color), and the hairpin cartoons depict the N, TS, and U structures. Notice that the hairpin's loop is formed at TS, and the unpaired strands form random coils at zero force. Our results agree with the thermodynamic features of DNA FELs studied using coarse-grained models. For example, in the OxDNA model, an initial sharp rise in free energy upon forming the first base pairs of the stem precedes the hybridization of the double-stranded DNA [79, 80].

The derived kinetic barriers to unfold, $\Delta G^{\ddagger} = \Delta H^{\ddagger} - T\Delta S^{\ddagger}$, and to fold, $\Delta G^{*} = \Delta H^{*} - T\Delta S^{*}$, at T_m are shown in Table 3 (third column) and their temperature dependences in Supplementary Fig. S7. Notice that $\Delta G^{\ddagger}_m \sim \Delta G^{*}_m$ as a consequence of the melting condition, $\Delta G_0(T_m) = \Delta G^{\ddagger}_m - \Delta G^{*}_m = 0$. Results show that $\Delta G^{\ddagger}(T) \gg \Delta G^{*}(T)$ with $\Delta G^{*}(T) \leq 5$ kcal/mol in the range 5–50°C. The nearly flat upper part of the funnel shown in Fig. 5C reflects the low $\Delta G^{*}(T)$, as predicted by the downhill-folding barrierless scenario [81–83].

Despite the different chemistry in nucleic acids and proteins, the common features in their folding thermodynamics are remarkable. In proteins, the nucleating precursor of N is a dry-molten globule whose formation is driven by the hydrophobicity of the core [6, 71]. In DNA hairpins, loop formation initiates the alignment of the unpaired strands at the stem's end. This nucleation step drives the zipping of the hairpin toward the formation of the stem duplex. Our study might be extended to RNAs with rougher energy landscapes that transiently form *misfoldons* upon folding [84–86] as well as to intermolecular DNA–ligand binding [87, 88].

Acknowledgements

Author contributions: Marc Rico-Pasto (Data curation [lead], Formal analysis [lead], Investigation [lead], Methodology [lead], Software [lead], Writing—original draft [equal], Writing—review & editing [equal]), Marco Ribezzi-Crivellari (Conceptualization [equal], Validation [equal], Writing—review & editing [equal]), and Felix Ritort (Conceptualization [lead], Funding acquisition [lead], Project administration [lead], Supervision [lead], Validation [lead], Writing—original draft [equal], Writing—review & editing [equal])

Supplementary data

Supplementary data is available at NAR online.

Conflict of interest

None declared.

Funding

M.R.-P. acknowledges financial support from the Juan de la Cierva Grant No. JDC2022-049996-I, and F.R. acknowledges financial support from the Icrea Academia Prize 2018 and 2023 (Catalan Government) and the Spanish Research Council Grant No. PID2022-139913NB-100 financed by MCIN/AEI /10.13039/501100011033. Funding to pay the Open Access publication charges for this article was provided by Icrea Academia Prize 2018 and 2023 (Catalan Government) and the Spanish Research Council Grant No. PID2022-139913NB-100.

Data availability

All data are available upon request to the corresponding author.

References

1. Simmel FC, Yurke B, Singh HR. Principles and applications of nucleic acid strand displacement reactions. *Chem Rev* 2019;**119**:6326–69. https://doi.org/10.1021/acs.chemrev.8b00580
2. Xiao S, Sharpe DJ, Chakraborty D *et al.* Energy landscapes and hybridization pathways for DNA hexamer duplexes. *J Phys Chem Lett* 2019;**10**:6771–9. https://doi.org/10.1021/acs.jpclett.9b02356
3. Juraszek J, Vreede J, Bolhuis PG. Transition path sampling of protein conformational changes. *Chem Phys* 2012;**396**:30–44. https://doi.org/10.1016/j.chemphys.2011.04.032
4. Frauenfelder H, Sligar SG, Wolynes PG. The energy landscapes and motions of proteins. *Science* 1991;**254**:1598–603. https://doi.org/10.1126/science.1749933
5. Bryngelson JD, Onuchic JN, Socci ND *et al.* Funnels, pathways, and the energy landscape of protein folding: a synthesis. *Prot Struct Funct Bioinform* 1995;**21**:167–95. https://doi.org/10.1002/prot.340210302
6. Rico-Pasto M, Zaltron A, Davis SJ *et al.* Molten globule-like transition state of protein barnase measured with calorimetric force spectroscopy. *Proc Natl Acad Sci USA* 2022;**119**:e2112382119. https://doi.org/10.1073/pnas.2112382119
7. Cooper A, Nutley MA, Wadood A. Differential scanning microcalorimetry. In: Harding SE, Chowdhry BZ (eds), *Protein–Ligand Interactions: Hydrodynamics and Calorimetry*. Oxford: Oxford University Press, 2000, 287–318. https://doi.org/10.1093/oso/9780199637492.003.0011
8. Freire E, Mayorga OL, Straume M. Isothermal titration calorimetry. *Anal Chem* 1990;**62**:950A–9A. https://doi.org/10.1021/ac00217a002
9. Marky LA, Breslauer KJ. Calorimetric determination of base-stacking enthalpies in double-helical DNA molecules. *Biopolymers* 1982;**21**:2185–94. https://doi.org/10.1002/bip.360211107
10. Breslauer KJ, Frank R, Blöcker H *et al.* Predicting DNA duplex stability from the base sequence. *Proc Natl Acad Sci USA* 1986;**83**:3746–50. https://doi.org/10.1073/pnas.83.11.3746
11. Vesnaver G, Breslauer KJ. The contribution of DNA single-stranded order to the thermodynamics of duplex formation. *Proc Natl Acad Sci USA* 1991;**88**:3569–73. https://doi.org/10.1073/pnas.88.9.3569
12. Holbrook JA, Capp MW, Saecker RM *et al.* Enthalpy and heat capacity changes for formation of an oligomeric DNA duplex: interpretation in terms of coupled processes of formation and association of single-stranded helices. *Biochemistry* 1999;**38**:8409–22. https://doi.org/10.1021/bi990043w
13. Tikhomirova A, Taulier N, Chalikian TV. Energetics of nucleic acid stability: the effect of Δ CP. *J Am Chem Soc* 2004;**126**:16387–94. https://doi.org/10.1021/ja046387d
14. Chalikian TV, Völker J, Plum GE *et al.* A more unified picture for the thermodynamics of nucleic acid duplex melting: a characterization by calorimetric and volumetric techniques. *Proc Natl Acad Sci USA* 1999;**96**:7853–8. https://doi.org/10.1073/pnas.96.14.7853
15. Vaitiekunas P, Crane-Robinson C, Privalov PL. The energetic basis of the DNA double helix: a combined microcalorimetric approach. *Nucleic Acids Res* 2015;**43**:8577–89. https://doi.org/10.1093/nar/gkv812
16. Rouzina I, Bloomfield VA. Heat capacity effects on the melting of DNA. 1. General aspects. *Biophys J* 1999;**77**:3242–51. https://doi.org/10.1016/S0006-3495(99)77155-9
17. Rouzina I, Bloomfield VA. Heat capacity effects on the melting of DNA. 2. Analysis of nearest-neighbor base pair effects. *Biophys J*

1999;**77**:3252–5. https://doi.org/10.1016/S0006-3495(99)77156-0
18. Mikulecky PJ, Feig AL. Heat capacity changes associated with DNA duplex formation: salt-and sequence-dependent effects. *Biochemistry* 2006;**45**:604–16. https://doi.org/10.1021/bi0517178
19. Breslauer KJ, Frank R, Blöcker H *et al.* Predicting DNA duplex stability from the base sequence. *Proc Natl Acad Sci USA* 1986;**83**:3746–50. https://doi.org/10.1073/pnas.83.11.3746
20. Mikulecky PJ, Feig AL. Heat capacity changes associated with nucleic acid folding. *Biopolymers* 2006;**82**:38–58. https://doi.org/10.1002/bip.20457
21. Frykholm K, Müller V, Sriram K *et al.* DNA in nanochannels: theory and applications. *Q Rev Biophys* 2022;**55**:e12. https://doi.org/10.1017/S0033583522000117
22. Hartmann A, Sreenivasa K, Schenkel M *et al.* An automated single-molecule FRET platform for high-content, multiwell plate screening of biomolecular conformations and dynamics. *Nat Commun* 2023;**14**:6511. https://doi.org/10.1038/s41467-023-42232-3
23. Agam G, Gebhardt C, Popara M *et al.* Reliability and accuracy of single-molecule FRET studies for characterization of structural dynamics and distances in proteins. *Nat Methods* 2023;**20**:523–35. https://doi.org/10.1038/s41592-023-01807-0
24. Collin D, Ritort F, Jarzynski C *et al.* Verification of the Crooks fluctuation theorem and recovery of RNA folding free energies. *Nature* 2005;**437**:231–4. https://doi.org/10.1038/nature04061
25. Alemany A, Mossa A, Junier I *et al.* Experimental free-energy measurements of kinetic molecular states using fluctuation theorems. *Nat Phys* 2012;**8**:688–94. https://doi.org/10.1038/nphys2375
26. Tapia-Rojo R, Mora M, Garcia-Manyes S. Single-molecule magnetic tweezers to probe the equilibrium dynamics of individual proteins at physiologically relevant forces and timescales. *Nat Protoc* 2024;**19**:1779–1806. https://doi.org/10.1038/s41596-024-00965-5
27. Kim E, Lee S, Jeon A *et al.* A single-molecule dissection of ligand binding to a protein with intrinsic dynamics. *Nat Chem Biol* 2013;**9**:313–8. https://doi.org/10.1038/nchembio.1213
28. Li Y, Qin M, Li Y *et al.* Single molecule evidence for the adaptive binding of DOPA to different wet surfaces. *Langmuir* 2014;**30**:4358–66. https://doi.org/10.1021/la501189n
29. Camunas-Soler J, Alemany A, Ritort F. Experimental measurement of binding energy, selectivity, and allostery using fluctuation theorems. *Science* 2017;**355**:412–5. https://doi.org/10.1126/science.aah4077
30. Woodside MT, Anthony PC, Behnke-Parks WM *et al.* Direct measurement of the full, sequence-dependent folding landscape of a nucleic acid. *Science* 2006;**314**:1001–4. https://doi.org/10.1126/science.1133601
31. Woodside MT, Behnke-Parks WM, Larizadeh K *et al.* Nanomechanical measurements of the sequence-dependent folding landscapes of single nucleic acid hairpins. *Proc Natl Acad Sci USA* 2006;**103**:6190–5. https://doi.org/10.1073/pnas.0511048103
32. Gupta AN, Vincent A, Neupane K *et al.* Experimental validation of free-energy-landscape reconstruction from non-equilibrium single-molecule force spectroscopy measurements. *Nat Phys* 2011;**7**:631–4. https://doi.org/10.1038/nphys2022
33. Woodside MT, Block SM. Reconstructing folding energy landscapes by single-molecule force spectroscopy. *Annu Rev Biophys* 2014;**43**:19–39. https://doi.org/10.1146/annurev-biophys-051013-022754
34. Manuel AP, Lambert J, Woodside MT. Reconstructing folding energy landscapes from splitting probability analysis of single-molecule trajectories. *Proc Natl Acad Sci USA* 2015;**112**:7183–8. https://doi.org/10.1073/pnas.1419490112
35. McCauley MJ, Rouzina I, Williams MC. Constructing free energy landscapes of nucleic acid hairpin unfolding. *DNA Nanotechnol Methods Protoc* 2018; **1811**:315–32. https://doi.org/10.1007/978-1-4939-8582-1_21
36. Bell GI. Models for the specific adhesion of cells to cells. *Science* 1978;**200**:618–27. https://doi.org/10.1126/science.347575
37. Evans E, Ritchie K. Dynamic strength of molecular adhesion bonds. *Biophys J* 1997;**72**:1541–55. https://doi.org/10.1016/S0006-3495(97)78802-7
38. Evans E. Probing the relation between force—lifetime—and chemistry in single molecular bonds. *Annu Rev Biophys Biomol Struct* 2001;**30**:105–28. https://doi.org/10.1146/annurev.biophys.30.1.105
39. Gebhardt JCM, Bornschlögl T, Rief M. Full distance-resolved folding energy landscape of one single protein molecule. *Proc Natl Acad Sci USA* 2010;**107**:2013–8. https://doi.org/10.1073/pnas.0909854107
40. Neupane K, Manuel AP, Lambert J *et al.* Transition-path probability as a test of reaction-coordinate quality reveals DNA hairpin folding is a one-dimensional diffusive process. *J Phys Chem Lett* 2015;**6**:1005–10. https://doi.org/10.1021/acs.jpclett.5b00176
41. Neupane K, Manuel AP, Woodside MT. Protein folding trajectories can be described quantitatively by one-dimensional diffusion over measured energy landscapes. *Nat Phys* 2016;**12**:700–3. https://doi.org/10.1038/nphys3677
42. Rico-Pasto M, Alemany A, Ritort F. Force-dependent folding kinetics of single molecules with multiple intermediates and pathways. *J Phys Chem Lett* 2022;**0**:1025–32. https://doi.org/10.1021/acs.jpclett.1c03521
43. Qu X, Smith GJ, Lee KT *et al.* Single-molecule nonequilibrium periodic Mg^{2+}-concentration jump experiments reveal details of the early folding pathways of a large RNA. *Proc Natl Acad Sci USA* 2008;**105**:6602–7. https://doi.org/10.1073/pnas.0801436105
44. Zhao R, Marshall M, Alemán EA *et al.* Laser-assisted single-molecule refolding (LASR). *Biophys J* 2010;**99**:1925–31. https://doi.org/10.1016/j.bpj.2010.07.019
45. Holmstrom ED, Nesbitt DJ. Single-molecule fluorescence resonance energy transfer studies of the human telomerase RNA pseudoknot: temperature-/urea-dependent folding kinetics and thermodynamics. *J Phys Chem B* 2014;**118**:3853–63. https://doi.org/10.1021/jp501893c
46. Meuzelaar H, Vreede J, Woutersen S. Influence of Glu/Arg, Asp/Arg, and Glu/Lys salt bridges on α-helical stability and folding kinetics. *Biophys J* 2016;**110**:2328–41. https://doi.org/10.1016/j.bpj.2016.04.015
47. Mao H, Ricardo Arias-Gonzalez J, Smith SB *et al.* Temperature control methods in a laser tweezers system. *Biophys J* 2005;**89**:1308–16. https://doi.org/10.1529/biophysj.104.054536
48. Stephenson W, Keller S, Santiago R *et al.* Combining temperature and force to study folding of an RNA hairpin. *Phys Chem Chem Phys* 2014;**16**:906–17. https://doi.org/10.1039/C3CP52042K
49. Rico-Pasto M, Zaltron A, Ritort F. Force dependence of proteins' transition state position and the Bell–Evans model. *Nanomaterials* 2021;**11**:3023–34. https://doi.org/10.3390/nano11113023
50. De Lorenzo S, Ribezzi-Crivellari M, Arias-Gonzalez JR *et al.* A temperature-jump optical trap for single-molecule manipulation. *Biophys J* 2015;**108**:2854–64. https://doi.org/10.1016/j.bpj.2015.05.017
51. Rico-Pasto M, Pastor I, Ritort F. Force feedback effects on single molecule hopping and pulling experiments. *J Chem Phys* 2018;**148**:123327. https://doi.org/10.1063/1.5010303
52. Forns N, de Lorenzo S, Manosas M *et al.* Improving signal/noise resolution in single-molecule experiments using molecular constructs with short handles. *Biophys J* 2011;**100**:1765–74. https://doi.org/10.1016/j.bpj.2011.01.071
53. Viader-Godoy X, Manosas M, Ritort F. Sugar-pucker force-induced transition in single-stranded DNA. *Int J Mol Sci* 2021;**22**:4745. https://doi.org/10.3390/ijms22094745

54. Buhot A, Halperin A. Effects of stacking on the configurations and elasticity of single-stranded nucleic acids. *Phys Rev E* 2004;**70**:020902. https://doi.org/10.1103/PhysRevE.70.020902
55. Seol Y, Skinner GM, Visscher K *et al.* Stretching of homopolymeric RNA reveals single-stranded helices and base-stacking. *Phys Rev Lett* 2007;**98**:158103. https://doi.org/10.1103/PhysRevLett.98.158103
56. Alemany A, Ritort F. Force-dependent folding and unfolding kinetics in DNA hairpins reveals transition-state displacements along a single pathway. *J Phys Chem Lett* 2017;**8**:895–900. https://doi.org/10.1021/acs.jpclett.6b02687
57. Bustamante C, Marko J, Siggia E *et al.* Entropic elasticity of lambda-phage DNA. *Science* 1994;**265**:1599–600. https://doi.org/10.1126/science.8079175
58. Rico-Pasto M, Ritort F. Temperature-dependent elastic properties of DNA. *Biophys Rep* 2022;**2**:100067. https://doi.org/10.1016/j.bpr.2022.100067
59. SantaLucia J. A unified view of polymer, dumbbell, and oligonucleotide DNA nearest-neighbor thermodynamics. *Proc Natl Acad Sci USA* 1998;**95**:1460–5. https://doi.org/10.1073/pnas.95.4.1460
60. Zuker M. Mfold web server for nucleic acid folding and hybridization prediction. *Nucleic Acids Res* 2003;**31**:3406–15. https://doi.org/10.1093/nar/gkg595
61. Goddard NL, Bonnet G, Krichevsky O *et al.* Sequence dependent rigidity of single stranded DNA. *Phys Rev Lett* 2000;**85**:2400. https://doi.org/10.1103/PhysRevLett.85.2400
62. McIntosh DB, Duggan G, Gouil Q *et al.* Sequence-dependent elasticity and electrostatics of single-stranded DNA: signatures of base-stacking. *Biophys J* 2014;**106**:659–66. https://doi.org/10.1016/j.bpj.2013.12.018
63. Kilchherr F, Wachauf C, Pelz B *et al.* Single-molecule dissection of stacking forces in DNA. *Science* 2016;**353**:aaf5508. https://doi.org/10.1126/science.aaf5508
64. Nicholas RM, Leslie SZ, Michael Z. UNAFold: Unified Nucleic Acid Folding and hybridization package. 1999.
65. Huguet JM, Bizarro CV, Forns N *et al.* Single-molecule derivation of salt dependent base-pair free energies in DNA. *Proc Natl Acad Sci USA* 2010;**107**:15431–6. https://doi.org/10.1073/pnas.1001454107
66. Huguet JM, Ribezzi-Crivellari M, Bizarro CV *et al.* Derivation of nearest-neighbor DNA parameters in magnesium from single molecule experiments. *Nucleic Acids Res* 2017;**45**:12921–31. https://doi.org/10.1093/nar/gkx1161
67. Segawa SI, Sugihara M. Characterization of the transition state of lysozyme unfolding. I. Effect of protein–solvent interactions on the transition state. *Biopolymers* 1984;**23**:2473–88. https://doi.org/10.1002/bip.360231122
68. Scalley ML, Baker D. Protein folding kinetics exhibit an Arrhenius temperature dependence when corrected for the temperature dependence of protein stability. *Proc Natl Acad Sci USA* 1997;**94**:10636–40. https://doi.org/10.1073/pnas.94.20.10636
69. Nguyen H, Jäger M, Moretto A *et al.* Tuning the free-energy landscape of a WW domain by temperature, mutation, and truncation. *Proc Natl Acad Sci USA* 2003;**100**:3948–53. https://doi.org/10.1073/pnas.0538054100
70. Hua L, Zhou R, Thirumalai D *et al.* Urea denaturation by stronger dispersion interactions with proteins than water implies a 2-stage unfolding. *Proc Natl Acad Sci USA* 2008;**105**:16928–33. https://doi.org/10.1073/pnas.0808427105
71. Baldwin RL, Frieden C, Rose GD. Dry molten globule intermediates and the mechanism of protein unfolding. *Prot Struct Funct Bioinform* 2010;**78**:2725–37. https://doi.org/10.1002/prot.22803
72. Jha SK, Marqusee S. Kinetic evidence for a two-stage mechanism of protein denaturation by guanidinium chloride. *Proc Natl Acad Sci USA* 2014;**111**:4856–61. https://doi.org/10.1073/pnas.1315453111
73. Ngai K, Yamamuro O. Thermodynamic fragility and kinetic fragility in supercooling liquids: a missing link in molecular liquids. *J Chem Phys* 1999;**111**:10403–6. https://doi.org/10.1063/1.480394
74. Rich A, Davies DR, Crick FHC *et al.* The molecular structure of polyadenylic acid. *J Mol Biol* 1961;**3**:71–86. https://doi.org/10.1016/S0022-2836(61)80009-0
75. Kauzmann W. The nature of the glassy state and the behavior of liquids at low temperatures. *Chem Rev* 1948;**43**:219–56. https://doi.org/10.1021/cr60135a002
76. Sastry S. The relationship between fragility, configurational entropy and the potential energy landscape of glass-forming liquids. *Nature* 2001;**409**:164–7. https://doi.org/10.1038/35051524
77. Muñoz V, Sanchez-Ruiz JM. Exploring protein-folding ensembles: a variable-barrier model for the analysis of equilibrium unfolding experiments. *Proc Natl Acad Sci USA* 2004;**101**:17646–51. https://doi.org/10.1073/pnas.0405829101
78. Berkovich R, Garcia-Manyes S, Klafter J *et al.* Hopping around an entropic barrier created by force. *Biochem Biophys Res Commun* 2010;**403**:133–7. https://doi.org/10.1016/j.bbrc.2010.10.133
79. Ouldridge TE, Louis AA, Doye JP. DNA nanotweezers studied with a coarse-grained model of DNA. *Phys Rev Lett* 2010;**104**:178101. https://doi.org/10.1103/PhysRevLett.104.178101
80. Ouldridge TE, Šulc P, Romano F *et al.* DNA hybridization kinetics: zippering, internal displacement and sequence dependence. *Nucleic Acids Res* 2013;**41**:8886–95. https://doi.org/10.1093/nar/gkt687
81. Garcia-Mira MM, Sadqi M, Fischer N *et al.* Experimental identification of downhill protein folding. *Science* 2002;**298**:2191–5.
82. Liu F, Du D, Fuller AA *et al.* An experimental survey of the transition between two-state and downhill protein folding scenarios. *Proc Natl Acad Sci USA* 2008;**105**:2369–74.
83. Sanstead PJ, Tokmakoff A. Direct observation of activated kinetics and downhill dynamics in DNA dehybridization. *J Phys Chem B* 2018;**122**:3088–100.
84. Rissone P, Bizarro CV, Ritort F. Stem–loop formation drives RNA folding in mechanical unzipping experiments. *Proc Natl Acad Sci USA* 2022;**119**:e2025575119. https://doi.org/10.1073/pnas.2025575119
85. Rissone P, Ritort F. Nucleic acid thermodynamics derived from mechanical unzipping experiments. *Life* 2022;**12**:1089.
86. Barciszewski J. *RNA Structure and Function*. Chan, Switzerland: Springer, 2023.
87. Riesenberg C, Iriarte-Valdez CA, Becker A *et al.* Probing ligand–receptor interaction in living cells using force measurements with optical tweezers. *Front Bioeng Biotechnol* 2020;**8**:598459.
88. Sánchez WN, Robeson L, Carrasco V *et al.* Determination of protein–protein interactions at the single-molecule level using optical tweezers. *Q Rev Biophys* 2022;**55**:e8.

Received: November 24, 2024. **Revised:** June 12, 2025. **Editorial Decision:** July 1, 2025. **Accepted:** July 7, 2025